

# Experimental Verification of Methane Replacement in Gas Hydrates by Carbon Dioxide

Yongwon Seo<sup>\*a</sup>, Seungmin Lee<sup>b</sup>, Jaehyoung Lee<sup>c</sup>

<sup>a</sup>School of Urban and Environmental Engineering, Ulsan National Institute of Science and Technology, Ulsan 689-798, Republic of Korea

<sup>b</sup>Offshore Plant Resources R&D Center, Korea Institute of Industrial Technology, Busan 618-230, Republic of Korea

<sup>c</sup>Petroleum & Marine Resources Division, Korea Institute of Geoscience & Mineral Resources, Daejeon 305-350, Republic of Korea

[ywseo@unist.ac.kr](mailto:ywseo@unist.ac.kr)

If the conversion of methane hydrate to carbon dioxide hydrate with the net recovery of methane could occur, this would be quite attractive as an innovative method of both methane production and carbon dioxide storage. In this study, the swapping phenomenon occurring in gas hydrates and its potential application to carbon dioxide sequestration was demonstrated through stability condition measurements and <sup>13</sup>C NMR spectroscopic analysis. The hydrate phase equilibria for the ternary CH<sub>4</sub> + CO<sub>2</sub> + water mixtures were measured to determine the hydrate stability conditions of the mixed gas hydrates. Through <sup>13</sup>C NMR measurements, it was found that carbon dioxide has a preference for the large cages in the sl hydrate and carbon dioxide is a relatively poorer guest when carbon dioxide competes with methane in occupying the small cages of the sl hydrate. From the NMR spectra and direct dissociation, it was confirmed that about 70% of methane is recoverable after reaction with carbon dioxide.

## 1. Introduction

Gas hydrates are solid inclusion compounds in which guest molecules of suitable size and shape are incorporated into hydrogen-bonded water frameworks. These compounds exist in three distinct crystal structures, sl, slI and sH, which consist of various cages with different sizes and shapes (Sloan and Koh, 2008). Gas hydrates are of particular interest in the gas and oil industry as well as in relation to greenhouse gas sequestration (Sloan and Koh, 2008). Naturally occurring gas hydrates, which contain mostly methane (CH<sub>4</sub>) and are found in the permafrost regions and deep ocean sediments, have great potential as future energy resources due to their huge quantities and wide geographical distribution (Sloan and Koh, 2008). Furthermore, carbon dioxide (CO<sub>2</sub>) produced from fossil fuel-fired power plants can be sequestered as solid gas hydrates in the deep ocean (Tajima et al., 2004). Recent investigations suggest the possibility of exchanging CH<sub>4</sub> with CO<sub>2</sub> in natural gas hydrates, which has the advantage of both CO<sub>2</sub> sequestration and CH<sub>4</sub> recovery (Hirohama et al., 1996; Lee et al., 2003; Park et al., 2006). Molecular dynamic simulations revealed that the substitution of CH<sub>4</sub> with CO<sub>2</sub> in sl hydrate cages has a negative free energy (Dorman, 2007). This indicates that CO<sub>2</sub> spontaneously replaces CH<sub>4</sub> from sl hydrates, causing the release of CH<sub>4</sub>. With the replacement of CH<sub>4</sub> with CO<sub>2</sub>, the naturally occurring gas hydrates can function as both CH<sub>4</sub> sources and CO<sub>2</sub> storage sites.

Several studies on the CH<sub>4</sub>-CO<sub>2</sub> swapping process, covering both spectroscopic and kinetic approaches, have recently been reported and have demonstrated notable success (Lee et al., 2003; Park et al., 2006). However, little attention has been paid to the complex phase behavior of the mixed CH<sub>4</sub>-CO<sub>2</sub> gas hydrates and its direct relation to guest distribution in CH<sub>4</sub>-CO<sub>2</sub> swapping. A complete understanding of the complex phase behavior and guest distribution is essential for revealing the CH<sub>4</sub>-CO<sub>2</sub> replacement mechanism. The phase behavior can offer stability conditions of the mixed gas hydrates and thus is very important in determining the pressure and temperature conditions of CO<sub>2</sub> being injected into the CH<sub>4</sub> hydrate layer. In addition, the guest distribution is closely related to the extent of CO<sub>2</sub> replacement in the CH<sub>4</sub> hydrate.

Therefore, in this study, the complex phase behavior of mixed CH<sub>4</sub>-CO<sub>2</sub> gas hydrates was intimately connected to <sup>13</sup>C NMR spectroscopic results in order to explore the guest distribution and the extent of CO<sub>2</sub> replacement and, furthermore, to reveal the CH<sub>4</sub>-CO<sub>2</sub> swapping mechanism. For this purpose, the three-phase equilibria (hydrate (H) – liquid water (L<sub>w</sub>) – vapor (V)) for ternary CH<sub>4</sub> + CO<sub>2</sub> + water mixtures were measured at CO<sub>2</sub> compositions of 20 and 60 % in order to meet changeable stability conditions in the CH<sub>4</sub>-CO<sub>2</sub> swapping process. Based on the three-phase equilibrium conditions, the pressure-composition diagram at a specified temperature was obtained in order to estimate the guest composition in the hydrate phase after swapping. Solid-state NMR spectroscopy was used to examine the distribution of CH<sub>4</sub> over the two cage sites of the mixed CH<sub>4</sub> + CO<sub>2</sub> hydrates. From the pressure-composition diagram linked to the distribution of CH<sub>4</sub> in the hydrate cages, the CO<sub>2</sub> concentration in the hydrate phase after replacement could be accurately predicted and was compared with the actual value measured by gas chromatography.

## 2. Experimental

The gas mixtures of CH<sub>4</sub> + CO<sub>2</sub> (20 and 60 %) were supplied by PSG Gas Co. (Republic of Korea). Double distilled deionized water was used. The experimental apparatus for the hydrate phase equilibria was specially designed to measure the hydrate dissociation pressures and temperatures accurately. The equilibrium cell was made of 316 stainless steel and had an internal volume of about 250 cm<sup>3</sup>. The cell content was vigorously agitated by an impeller-type stirrer. The experiment for hydrate-phase equilibrium measurements began by charging the equilibrium cell with about 80 cm<sup>3</sup> of ultra high purity water. After the equilibrium cell was pressurized to the desired pressure with gas mixtures of CH<sub>4</sub> + CO<sub>2</sub>, the main system was slowly cooled to a temperature lower than the expected equilibrium value. Due to thermal contraction, the cell pressure was slightly decreased by decreasing the temperature at a cooling rate of 1 K /h. An abrupt pressure depression was subsequently observed at the stage of hydrate crystal growth after nucleation. When the pressure depression due to hydrate formation reached a steady-state condition, the temperature was increased in 0.1 K increments with sufficient time of 90 min, and accordingly, the cell pressure increased with gas hydrate dissociation. After all the hydrates were dissociated with increasing temperature, the cell pressure again increased slightly due to thermal expansion. The three-phase (H – L<sub>w</sub> – V) equilibrium points at each vapor composition were determined as the intersection between the hydrate dissociation and thermal expansion lines.

To measure the compositions of the vapor and hydrate phases, a sampling valve (Rheodyne, Model 7010, USA) with a loop volume of 20 μl was installed and connected to a gas chromatograph (Agilent 7890, USA) through a high-pressure metering pump (Eldex, USA). A thermal conductivity detector (TCD) and a Porapak Q column (Supelco, USA) were used as the detector and the column, respectively. For each experimental run, after nucleation, the equilibrium cell with an excess of water and vigorous agitation was left for 24 h to reach a state of equilibrium at a specified temperature. The vapor phase composition was then analyzed by gas chromatography, after the vapor phase was circulated through a sampling line with a high-pressure metering pump to equilibrate both compositions of the cell and loop for more than 10 min. The corresponding composition of the hydrate phase was also measured by gas chromatography after the vapor phase was evacuated under cooling of the cell in a liquid nitrogen vessel, and the entire hydrate phase was then dissociated at 298.15 K.

A Bruker 400 MHz solid-state NMR spectrometer was used to identify the hydrate structure and guest distributions in the mixed CH<sub>4</sub> + CO<sub>2</sub> hydrates. The NMR spectra were recorded at 243 K and atmospheric pressure by placing the clathrate hydrate samples in a 4 mm o.d. Zr rotor that was loaded into a variable-temperature (VT) probe. All <sup>13</sup>C NMR spectra were recorded at a Larmor frequency of 100.6 MHz with magic angle spinning (MAS) between 2 and 4 kHz. A pulse length of 2 μs and pulse repetition delay of 10 s under proton decoupling were employed when a radio frequency field strength of 50 kHz corresponding to 5 μs 90° pulses was used. The downfield carbon resonance peak of adamantane, which was assigned a chemical shift of 38.3 ppm at 300 K, was used as an external chemical shift reference. More detailed description of the experimental methods can be found in previous papers (Cha et al., 2010; Lee et al., 2012).

## 3. Results and Discussion

The three-phase H – L<sub>w</sub> – V equilibria for ternary CH<sub>4</sub> + CO<sub>2</sub> + water mixtures with two different CO<sub>2</sub> concentrations of 20 and 60 % were experimentally measured in order to understand the complex phase behavior of the mixed gas hydrates and to meet changeable stability conditions of the CH<sub>4</sub>-CO<sub>2</sub> swapping process. The equilibrium measurements for the mixed gas hydrates were undertaken over wide

temperature and pressure ranges, depending on the vapor phase  $\text{CO}_2$  concentrations and the results are presented in Figure 1. The H – L<sub>W</sub> – V lines of the ternary  $\text{CH}_4 + \text{CO}_2 + \text{water}$  mixtures exist between those of the binary  $\text{CH}_4 + \text{water}$  and  $\text{CO}_2 + \text{water}$  mixtures. Both  $\text{CH}_4$  and  $\text{CO}_2$  are known to form sl hydrates and to occupy both small and large cages of the hydrate structure (Sloan and Koh, 2008). However, due to the relatively larger molecular size of  $\text{CO}_2$ ,  $\text{CO}_2$  hydrate is thermodynamically more stable than  $\text{CH}_4$  hydrate, and accordingly, the H – L<sub>W</sub> – V lines of the  $\text{CH}_4 + \text{CO}_2 + \text{water}$  mixtures generally appear nearer to that of the binary  $\text{CO}_2 + \text{water}$  mixture than that of the binary  $\text{CH}_4 + \text{water}$  mixture.

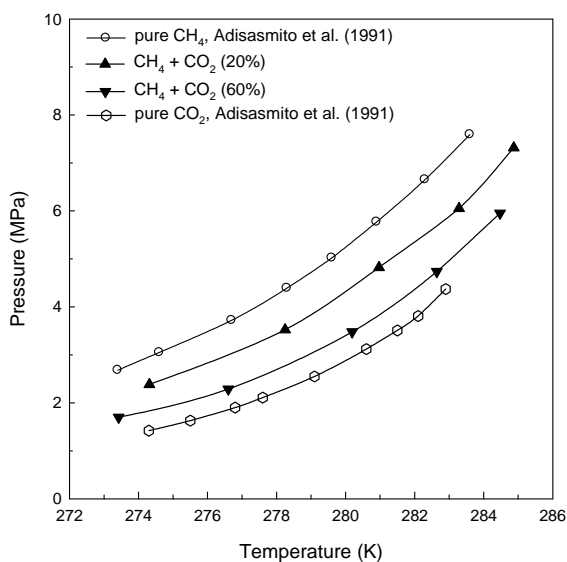


Figure 1. Gas hydrate phase equilibria of the  $\text{CH}_4 + \text{CO}_2 + \text{water}$  mixtures

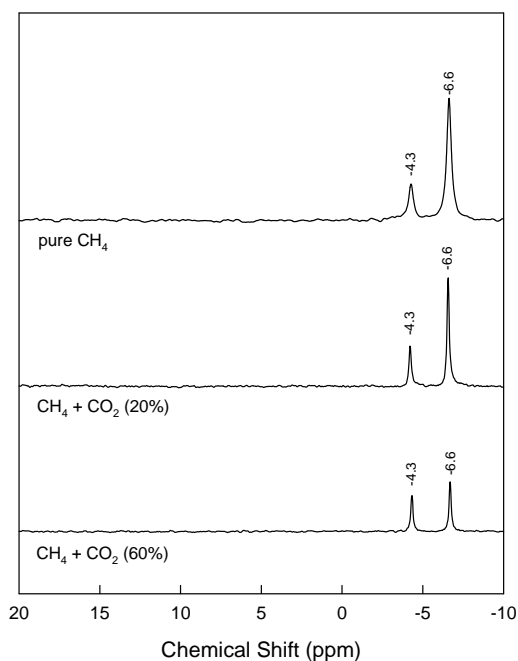


Figure 2.  $^{13}\text{C}$  MAS NMR spectra of sl hydrates prepared using  $\text{CH}_4 + \text{CO}_2$  gas mixtures

The pure  $\text{CH}_4$  hydrate and mixed  $\text{CH}_4 + \text{CO}_2$  hydrates were analyzed via  $^{13}\text{C}$  MAS NMR in order to investigate guest distributions and preferential occupation of each guest in the hydrate cages. The cage dependent  $^{13}\text{C}$  MAS NMR chemical shift for captured  $\text{CH}_4$  molecules can be effectively used to determine

the structure types of the mixed gas hydrate formed and to examine the distribution of CH<sub>4</sub> over the two different cage sites (Ripmeester and Ratcliffe, 1999). Figure 2 shows a stacked plot of the <sup>13</sup>C MAS NMR spectra of the pure CH<sub>4</sub> hydrate and CH<sub>4</sub> + CO<sub>2</sub> hydrates with two different CO<sub>2</sub> compositions (20 and 60%). The spectrum of the pure CH<sub>4</sub> hydrate, known to form sl hydrate, has two signals at -4.3 and -6.6 ppm. The peak at -4.3 ppm can be assigned to CH<sub>4</sub> molecules captured in the small 5<sup>12</sup> cages and the peak at -6.6 ppm to CH<sub>4</sub> molecules in the large 5<sup>12</sup>6<sup>4</sup> cages, considering the ideal stoichiometric ratio (1 : 3) of the small 5<sup>12</sup> to the large 5<sup>12</sup>6<sup>4</sup> cages in the unit cell of the sl. With increasing CO<sub>2</sub> concentration in the gas mixture, the peak area at -6.6 ppm relatively declines. The decrease in the peak area ratio with increasing CO<sub>2</sub> is attributed to the preferential occupation of CO<sub>2</sub> in the large 5<sup>12</sup>6<sup>4</sup> cages due to the difference in the molecular size of CH<sub>4</sub> and CO<sub>2</sub>. The molecular diameter of CO<sub>2</sub> is larger than that of CH<sub>4</sub> and is almost identical to the cavity diameter of the 5<sup>12</sup> cages in the sl hydrate (Sloan and Koh, 2008). Therefore, when CO<sub>2</sub> competes with CH<sub>4</sub> for occupying the small 5<sup>12</sup> cages, CO<sub>2</sub> is a relatively poorer guest for the 5<sup>12</sup> cages even though CO<sub>2</sub> can also occupy both small and large cages of the sl hydrate. The lower fractional occupancy of CO<sub>2</sub> in the small 5<sup>12</sup> cages results in a higher hydration number (CO<sub>2</sub>·6.3H<sub>2</sub>O) when compared with the hydration number of CH<sub>4</sub> hydrates (CH<sub>4</sub>·6.0H<sub>2</sub>O) (Sloan and Koh, 2008).

Figure 3 presents the <sup>13</sup>C MAS NMR spectra of the pure CH<sub>4</sub> hydrate (before replacement) and the mixed CH<sub>4</sub> + CO<sub>2</sub> hydrate (after replacement). In the <sup>13</sup>C MAS NMR spectra presented in Figure 3, the peak areas at -4.3 and -6.6 ppm are quantitatively proportional to the amount of CH<sub>4</sub> molecules captured in the small 5<sup>12</sup> and the large 5<sup>12</sup>6<sup>4</sup> cages, respectively. The area ratio of CH<sub>4</sub> molecules in large and small cages (A<sub>L</sub>/A<sub>S</sub>) for the pure CH<sub>4</sub> hydrate is 3.27, which indicates the hydrate composition of CH<sub>4</sub>·6.03H<sub>2</sub>O. Meanwhile, the A<sub>L</sub>/A<sub>S</sub> for the mixed gas hydrate after CO<sub>2</sub> replacement is 1.44, which is clearly caused by predominant occupation of CO<sub>2</sub> in the large 5<sup>12</sup>6<sup>4</sup> cages.

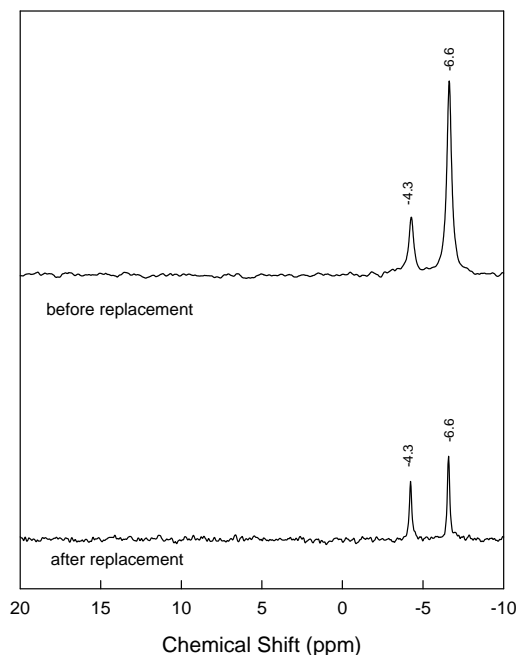


Figure 3. <sup>13</sup>C MAS NMR spectra of a sl hydrate before and after CO<sub>2</sub> replacement

From Figure 2, it can be found that the A<sub>L</sub>/A<sub>S</sub> value of 1.44, which results from CO<sub>2</sub> replacement, corresponds to a feed CO<sub>2</sub> concentration of 60 %. If this value of the feed CO<sub>2</sub> concentration is applied to the pressure-composition diagram shown in Figure 4, the corresponding CO<sub>2</sub> composition in the hydrate phase can be predicted. In Figure 4, the equilibrium CO<sub>2</sub> compositions of the hydrate and vapor phases, which were experimentally measured at 276.15 K, are depicted with calculation results. Compositions and cage occupancies of each component at equilibrium were calculated in the process of predicting equilibrium pressure at a specified temperature.

The equilibrium criteria of the hydrate-forming mixture are based on the equality of fugacities of the specified component *i* in all phases that coexist simultaneously

$$\hat{f}_i^H = \hat{f}_i^L = \hat{f}_i^V (= f_w^I) \quad (1)$$

where  $H$  denotes for the hydrate phase,  $L$  for the water-rich liquid phase,  $V$  for the vapor phase, and  $I$  for the ice phase.

In the model given here, for hydrate equilibrium calculations, the fugacities are calculated by SRK-EOS (Soave-Redlich-Kwong equation of state) incorporated with the modified Huron-Vidal second order mixing rule for fluid phases, and by statistical thermodynamics for the hydrate phase at the same pressure. The optimized Kihara potential parameters used in this study and more details of the model description were given in previous papers (Seo et al., 2002).

In the case of a feed  $\text{CO}_2$  concentration of 60%, the corresponding  $\text{CO}_2$  composition in the hydrate phase is 67% at 2.2 MPa as can be predicted from Figure 4. Here, 67%  $\text{CO}_2$  in the hydrate phase means that 67% recovery of  $\text{CH}_4$  can be achieved with  $\text{CO}_2$  injection into the  $\text{CH}_4$  hydrates. Assembling the results presented here, the  $A_L/A_S$  ratio of 1.44 after  $\text{CO}_2$  replacement derived from Figure 3 implies that approximately 67% of  $\text{CH}_4$  in the hydrate was replaced by  $\text{CO}_2$ . This is consistent with a previous result that at least 64% of  $\text{CH}_4$  should be recoverable by replacement of  $\text{CO}_2$  (Lee et al., 2003). In addition, the result is also almost identical to the  $\text{CO}_2$  composition of  $68 \pm 2\%$  which was measured directly by dissociation of the replaced hydrate sample. Based on both hydrate phase compositions and cage occupancy of each guest calculated from the combination of  $^{13}\text{C}$  NMR spectra, pressure-composition relation, and phase equilibrium modeling, the chemical formula for the mixed gas hydrate after  $\text{CO}_2$  replacement was found to be  $5.03\text{CO}_2 \cdot 2.51\text{CH}_4 \cdot 46\text{H}_2\text{O}$ .

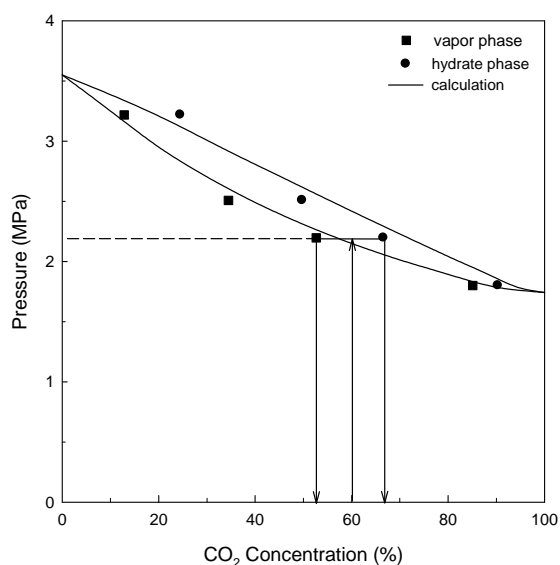


Figure 4. Pressure-composition diagram for the  $\text{CH}_4 + \text{CO}_2 + \text{water}$  mixtures at 276.15 K

#### 4. Conclusions

In this study, the replacement of  $\text{CH}_4$  by  $\text{CO}_2$  in naturally occurring gas hydrates was investigated as an innovative and efficient method of both sequestering a global warming gas and harvesting a future energy source. The experimental results presented here indicate that at least, in a laboratory setting, the replacement of  $\text{CH}_4$  by  $\text{CO}_2$  is favored and thus,  $\text{CO}_2$  is possibly sequestered into the  $\text{CH}_4$  hydrate layer. In particular, through thermodynamic equilibrium studies linked to the spectroscopic approach on replacement of  $\text{CH}_4$  by  $\text{CO}_2$ , the  $\text{CO}_2$  composition in the hydrate phase and the chemical formula of the mixed gas hydrate after replacement can be easily estimated if the information about the area ratio of the  $^{13}\text{C}$  MAS NMR resonance lines of  $\text{CH}_4$  molecules in large and small cages is provided. However, for actual  $\text{CO}_2$  replacement in natural gas hydrate deposits, a variety of factors such as reaction kinetics, sediment environment, mass transfer, and hydrate particle size should be further considered.

**References**

- Adisasmito, S.; Frank, R. J.; Sloan, E. D. 1991, Hydrates of carbon dioxide and methane mixtures. *J. Chem. Eng. Data*, 36, 68-71.
- Cha, I.; Lee, S.; Lee, J. D.; Lee, G.-W.; Seo, Y. 2010, Separation of SF<sub>6</sub> from gas mixtures using gas hydrate formation. *Environ. Sci. Technol.*, 44, 6117-6122.
- Dornan, P.; Alavi, S.; Woo, T. K. 2007, Free energies of carbon dioxide sequestration and methane recovery in clathrate hydrates. *J. Chem. Phys.*, 127, 124510.
- Hirohama, S.; Shimoyama, Y.; Wakabayashi, A.; Tatsuya, S.; Nishida, N. 1996, Conversion of CH<sub>4</sub>-hydrate to CO<sub>2</sub>-hydrate in liquid CO<sub>2</sub>. *J. Chem. Eng. Jpn.*, 29, 1014-1020.
- Lee, H.; Seo, Y.; Seo, Y.-T.; Moudrakovski, I.; Ripmeester, J. A. 2003, Recovering methane from solid methane hydrate with carbon dioxide. *Angew. Chem. Int. Ed.*, 42, 5048-5051.
- Lee, S.; Lee, Y.; Park, S.; Kim, Y.; Lee, J. D.; Seo, Y. 2012, Thermodynamic and spectroscopic identification of guest gas enclathration in the double tetra-n-butylammonium fluoride semiclathrates. *J. Phys. Chem. B*, 116, 9075-9081.
- Park, Y.; Kim, D.-Y.; Lee, J.-W.; Huh, D.-G.; Park, K.-P.; Lee, J.; Lee, H. 2006, Sequestering carbon dioxide into complex structures of naturally occurring gas hydrates. *Proc. Natl. Acad. Sci. USA*, 103, 12690-12694.
- Ripmeester, J.A.; Ratcliffe, C.I. 1999, On the contributions of NMR spectroscopy to clathrate science. *J. Struct. Chem.*, 40, 654-662.
- Seo, Y.; Lee, H.; Uchida, T. 2002, Methane and carbon dioxide hydrate phase behavior in small porous silica gels: three-phase equilibrium determination and thermodynamic modeling. *Langmuir*, 18, 9164-9170.
- Sloan, E. D.; Koh, C. A. 2008, *Clathrate Hydrates of Natural Gases*, 3rd Ed.; CRC Press: Boca Raton, U.S.A.
- Tajima, H.; Yamasaki, A.; Kiyono, F. 2004, Continuous formation of CO<sub>2</sub> hydrate via a kenics-type static mixer. *Energy Fuels*, 18, 1451-1456.